COMMUNICATION

Check for updates

Highly stretchable and self-healing photoswitchable supramolecular fluorescent polymers for underwater anti-counterfeiting†

Haitao Deng,[a] Hong Wang, [iD][a] Yong Tian,[a] Zhong Lin,[a] Jiaxi Cui [iD] *[b] and Jian Chen [iD] *[a]

Thanks to the non-destructiveness and spatial-controllability of light, photoswitchable fluorescent polymers (PFPs) have been successfully applied in advanced anti-counterfeiting and information encryption. However, most of them are not suitable for use in harsh underwater environments, including high salinity seawater. In this study, by integrating photochromic molecules into a hydrophobic polymer matrix with the fluorine elastomer, including dipole–dipole interactions, we describe a class of novel photoswitchable supramolecular fluorescent polymers (PSFPs) that can adaptively change their fluorescence between none, green and red by the irradiation of different light. The PSFPs not only exhibited excellent photoswitchable properties, including fast photo-responsibility, prominent photo-reversibility, and photostability, but also exhibited some desired properties, including exceptional stretchability, hydrophobicity, antifouling, self-healing ability, simple preparation process, and processability. We thus demonstrated their applications in underwater data encryption and anti-counterfeiting labels.

New concepts

Photoswitchable fluorescent polymers are often designed for advanced anti-counterfeiting and information encryption. These applications often involve harsh underwater environments (acid, base, or seawater), wherein traditional strategies for mechanical strengthening and self-healing normally fail due to the aqueous conditions. Dipole–dipole interactions are hydrophobic and expected to bring about self-healing ability even in an underwater environment. Herein, we demonstrate this concept by photoswitchable supramolecular fluorescent polymers crosslinked by dipole–dipole interactions. These materials combine the excellent photoswitchable properties of diarylethene derivatives and the dynamic properties of the supramolecular materials, resulting in an excellent overall performance. We evidence their applicability in underwater data encryption and anti-counterfeiting labels. They may be promising next-generation photoswitchable materials for underwater anti-counterfeiting labels and encryption.

Introduction

Nowadays, the development of the marine economy has become more and more important, which inevitably involves underwater anti-counterfeiting and encryption in some important or high value-added equipment.[1,2] Creating underwater anti-counterfeiting and encryption with high-level safety is very

necessary to prevent imitation or reproduction without the permission of the owner and avoid unnecessary economic losses.[3,4] By learning from organisms in nature, many stimulus-responsive (*e.g.*, light, temperature, pH, metal ion, mechanical force, and so on) polymer systems with alterable fluorescence emission have been developed to apply in anti-counterfeiting and encryption.[5–8] Among them, thanks to the non-destructiveness and spatial-controllability of light, light-driven photochromic molecules were integrated into polymer systems to create photoswitchable fluorescent polymers (**PFPs**) and applied in photorewritable patterns, anti-counterfeiting, and information encryption.[9–16] Recent reported **PFPs** are mainly based on nanoparticles, films, and hydrogels. However, nanoparticles possess poor mechanical properties due to the independent nanostructure.[17–20] Films and hydrogels cannot easily realize self-healing in harsh underwater environments (acid, base, or seawater).[21–27] Films containing supramolecular interactions (*e.g.*, H-bond, ionic interaction, host–guest interactions) and hydrogels can also be abnormally swelled or deswelled in acid, base, or high-concentration salt solutions,

[a] *Key Laboratory of Theoretical Organic Chemistry and Functional Molecule of Ministry of Education, Hunan Provincial Key Laboratory of Controllable Preparation and Functional Application of Fine Polymers, Hunan Provincial Key Lab of Advanced Materials for New Energy Storage and Conversion, Hunan Province College Key Laboratory of QSAR/QSPR, School of Chemistry and Chemical Engineering, Hunan University of Science and Technology, Xiangtan, Hunan 411201, China. E-mail: cj0066@gmail.com*

[b] *Institute of Fundamental and Frontier Sciences, University of Electronic Science and Technology of China, Chengdu 610054, China. E-mail: jiaxi.cui@uestc.edu.cn*

† Electronic supplementary information (ESI) available. See DOI: https://doi.org/10.1039/d3mh01239e

resulting in poor stability.[28–33] These disadvantages greatly limit their application. Therefore, it is highly desirable to develop **PFPs** with well-pleasing overall performance, including photoswitchable properties, antifouling, and self-healing ability for extending their application in humid environments and even seawater.

Supramolecular materials consisting of supramolecular interactions (*e.g.*, hydrogen bonds, ionic interaction, host–guest interactions, coordination complex, hydrophobic association, π–π stacking interaction) show many eminent characteristics, such as processability, self-healing ability, recyclability, *etc.*[34–43] In the last two decades, these materials have been applied to anti-counterfeiting, information encryption, self-healing, functional coatings, soft robots, *etc.*[44–51] However, these materials are still far away from applications in some special environments, such as underwater anti-counterfeiting and encryption, due to their poor stability and self-healing capability in harsh environments (high salt, strong acid–base environment). To address this issue, Wang *et al.* developed a new supramolecular system with dipole–dipole interactions, which exhibited remarkable stability in harsh aqueous environments and self-healable capability.[52] Therefore, introducing dipole–dipole interactions into polymer systems to create **PFPs** with self-healing capability is very necessary for meeting the criteria required for underwater anti-counterfeiting labels and encryption.

Herein, we report a class of new photoswitchable supramolecular fluorescent polymers (**PSFPs**) with excellent stability and self-healable capability in harsh aqueous environments *via* the facile copolymerization of diarylethylene derivatives (BTBA, SDTE), 2,2,2-trifluoroethyl methacrylate (TFEMA) and 2,2,3,4,4,4-hexafluorobutyl acrylate (HFBA). In our system, **PSFPs** have unique dipole–dipole interactions based on strong molecular dipoles, ensuring that the **PSFPs** not only show remarkable photoreversibility, photostability, and easy preparation, but also exhibit stretchability, hydrophobicity, antifouling, exceptional environmental stability including salt, acid and alkali resistance, and self-healing. These characteristics allow us to apply **PSFPs** in underwater adaptive discoloration, anti-counterfeiting, and information encryption.

Results and discussion

Fig. 1 shows our design. We chose the photoswitchable diarylethylene derivatives as a photochromic molecule and fluorescence resonance energy transfer (FRET) donor (SDTE-c) and acceptor (BTBA-c) to integrate into the hydrophobic fluorine elastomer including dipole–dipole interactions for the development of **PSFPs**. The fluorescence of **PSFPs** can be reversibly altered between none, green and red (Fig. 1a and 1b).[53] Briefly, UV2 (254 nm) could not only induce the structure transformation of SDTE from non-fluorescence to green fluorescence, but also cause the structure transformation of BTBA from non-fluorescence to red fluorescence. Vis2 (460 nm) could cause an opposite change. However, the BTBA can be reversibly switched
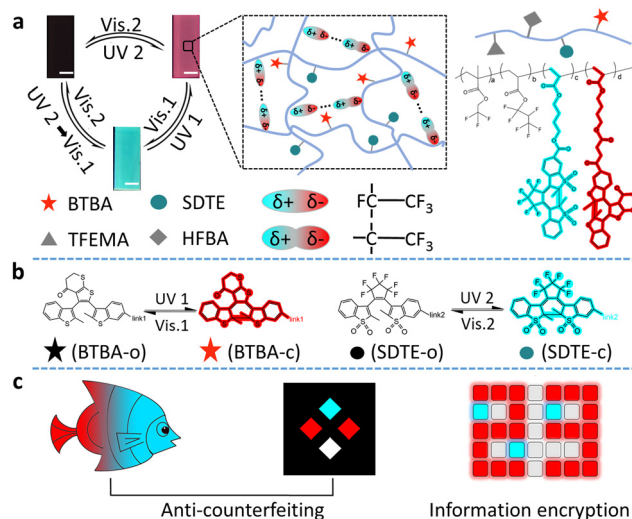

Fig. 1 Concept and preparation of PSFPs. (a) Schematic illustrations of the design strategy from two photochromic fluorescent monomers to a photoswitchable multistate fluorescent polymer, and dipole–dipole interactions based on a strong molecular dipole. Scale bar: 1.0 cm. (b) Schematic diagram of light-induced reversible structural transformation of BTBA and SDTE (non-emission, red and green). UV1: 365 nm; Vis1: 525 nm; UV2: 254 nm; Vis2: 460 nm. (c) Schematic illustration of an example underwater application (anti-counterfeiting, information encryption).

between non-fluorescence and red fluorescence using UV1 (365 nm) and Vis1 (525 nm) to stimulate alternately. In addition, dipole–dipole interactions make **PSFPs** have processability, hydrophobicity, antifouling, and self-healing ability.[54–56] Finally, the as-prepared **PSFPs** possess both photoswitchable properties and a well-pleasing comprehensive performance. Therefore, thanks to the non-destructiveness and spatial-controllability of light, we could use **PSFPs** as the desired tools to apply for underwater anti-counterfeiting and information encryption (Fig. 1c).

The two diarylethylene derivatives (BTBA, SDTE) were first synthesized based on our previous work.[53] The ring-closed state of SDTE-c exhibited an obvious absorbance peak (410 nm) and green fluorescence emission (500 nm) in tetrahydrofuran (THF), which was served as the FRET donor. The ring-closed state of BTBA-c exhibited an obvious absorbance peak (564 nm) and red fluorescence emission (655 nm) in THF, which was used as the FRET acceptor. Thereafter, **PSFPs** (**P3**) were synthesized by the light-induced free radical polymerization of the two diarylethylene derivatives (BTBA, SDTE), 2,2,2-trifluoroethyl methacrylate (TFEMA), and 2,2,3,4,4,4-hexafluorobutyl acrylate (HFBA, Fig. S4, ESI†). Other copolymers (**P0**, **P1**, **P2**) were synthesized (Fig. S1–S3 and Table S1, ESI†). The absorbance and fluorescence spectra of **P1**, **P2**, and **P3** indicated the successful copolymerization of TFEMA, HFBA, BTBA, and SDTE. The obtained polymers with moderate molecular weights (**P0**, M_n = 31.5 kDa; **P1**, M_n = 32.9 kDa; **P2**, M_n = 31.7 kDa; **P3**, M_n = 27.4 kDa, Table S1, ESI†) further demonstrated that the monomers were converted into copolymers. Because of the

reversibly photoswitchable performance of SDTE and BTBA and the effective FRET process between ring-closed SDTE-c (donor) and ring-closed BTBA-c (acceptor), the obtained **PSFPs** (**P3**) can be reversibly switched among three distinct states (non-emission, green, and red) under different light stimuli (Fig. 1a). In addition, due to the combination of TFEMA and HFBA containing CF_3 dipoles (Fig. 1a), the **PSFPs** existed unique dipole–dipole interactions based on a strong molecular dipole.[57] Furthermore, the glass transition temperatures (T_g) of these polymers (**P0**, $T_g = 18.25\ °C$; **P1**, $T_g = 19.82\ °C$; **P2**, $T_g = 20.07\ °C$; **P3**, $T_g = 21.02\ °C$, Fig. S5, ESI†) illustrated that the introduction of BTBA and SDTE could enhance the T_g. These low T_g endowed the polymer materials with eminent processability.[58]

With **PSFPs** in our hands, the optimal excitation wavelength was first investigated. Selecting the optimum wavelength as the excitation light can effectively avoid the test error caused by the excitation light in a photoswitchable material. Therefore, **P1** and **P2** were exposed to UV light (254 nm) for 5 min to obtain **P1** with red fluorescence emission and **P2** with green fluorescence emission, respectively. Subsequently, the **P1** with red fluorescence and **P2** with green fluorescence were excited by 410 nm light. The results showed that the fluorescence intensity of **P1** and **P2** exhibited a slight reduction ($<10\%$) even after continuous illumination for 30 min (Fig. S6, ESI†), indicating the photostability of the ring-closed state of BTBA-c and SDTE-c. Hence, 410 nm was chosen as the excitation wavelength for subsequent tests.

Next, we explored the photoswitching properties of **PSFPs**. As shown in Fig. 2a, the fluorescence of **P1** containing BTBA can be reversibly changed between red emission and non-emission states by alternately using 365 nm UV and 525 nm visible light to irradiate samples (Fig. 2a and Fig. S7a, ESI†). **P2** containing SDTE also revealed a similar change between green emission and non-emission states under UV (254 nm) and Vis (460 nm) light irradiation (Fig. 2b and Fig. S7b, ESI†). No significant fluorescence attenuation in **P1** and **P2** was noted during the 20 tests (Fig. S7c and S7d, ESI†), demonstrating that **P1** and **P2** presented satisfactory photo-reversibility. They also exhibited satisfying thermostability within 24 h (25 °C and 65 °C, Fig. S8a–d, ESI†) and long-term stability within 4 weeks (Fig. S8d and S8e, ESI†). As depicted in Fig. 2c and d and Fig. S9 (ESI†), **P3** displayed a reversible change between non-fluorescence, red fluorescence, and green fluorescence. Importantly, any two states are completely reversible (Fig. 2d). In addition, due to the overlap between the emission spectrum of SDTE-c units and the absorption spectrum of BTBA-c units (Fig. S10, ESI†), the obviously photo-controlled FRET process between SDTE-c and BTBA-c was achieved by utilizing Vis (525 nm) and UV (365 nm) to irradiate alternately the sample. As shown in Fig. 2e, when **P3** was translated to red fluorescence using UV (254 nm, FRET efficiency: 94.8%), upon the increase of the time of irradiation of Vis1, the red fluorescence was gradually turned to green fluorescence (Fig. 2f, and Fig. S11, ESI†). Subsequently, when green-fluorescent **P3** was further exposed to UV1 (365 nm), a decreased fluorescence quantum
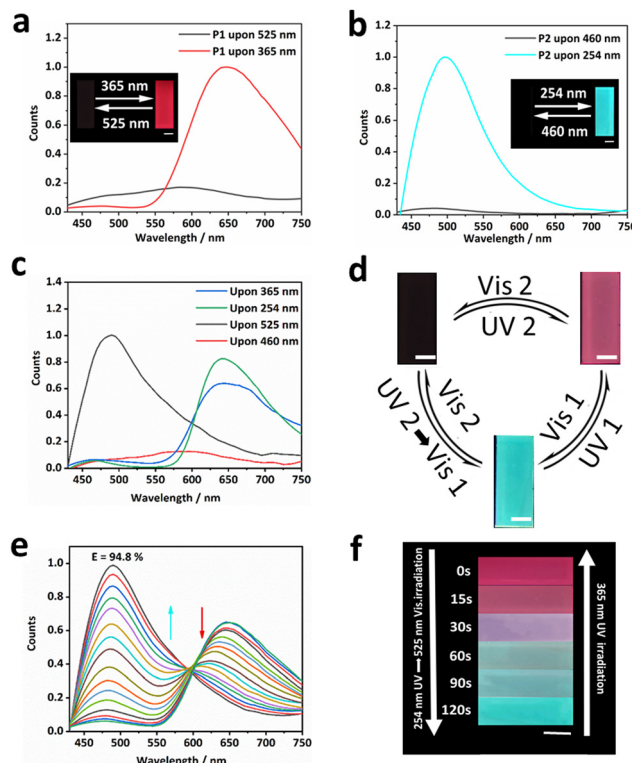
Fig. 2 Photoswitchable property. (a) Fluorescence emission of **P1** under different light irradiation (365 nm, 2.36 mW cm^{-2}, 4 min; 525 nm, 30 mW cm^{-2}, 6 min). Inset in (a): Optical photographs of **P1** under UV1 and Vis1. (b) Fluorescence emission of **P2** under different light irradiation (254 nm, 2.8 mW cm^{-2}, 5 min; 460 nm, 40 mW cm^{-2}, 3 min). Inset in (b): Optical photographs of **P2** under UV2 and Vis2. (c) Fluorescence emission of **P3** under the illumination of different light (365 nm, 5 min; 254 nm, 4 min; 525 nm, 6 min; 460 nm, 3 min). (d) Fluorescence variation of the **P3** film after irradiation with different UV (UV1 and UV2) and Vis (Vis1 and Vis2). (e) The fluorescence response of the BTBA unit in the **P3** membrane under 365 and 525 nm irradiation, $\lambda_{ex} = 410$ nm. (f) The graphs of the **P3** film upon 365 nm, 254 nm and 525 nm irradiation, fluorescence observed under a 365 nm lamp. All scale bars are 1.0 cm. All fluorescence images were observed under a 365 nm UV lamp.

yield (3.26% to < 0.01%, $\lambda_{ex} = 410$ nm, $\lambda_{em} = 430$–550 nm, Table S2, ESI†) and fluorescence lifetime (3.6 ns to 2.6 ns, Fig. S12, ESI†) indicated that a FRET process between SDTE-c (donor) and BTBA-c (acceptor) occurred. The multi-wavelength response is very conducive to creating highly secure information encryption and anti-counterfeiting labels.

The polymer matrixes exhibited typical supramolecular interactions (dipole–dipole interactions) based on a strong molecular dipole (Fig. 1c). These dynamic interactions endow **PSFPs** (**P0**) with high moduli (196 MPa), typical yielding points (0.51 MPa), strength (0.38 MPa), and moderate stretchability (15.5 times strain) (Fig. 3a). In addition, **PSFPs** can achieve highly efficient self-healing because of the existence of a large number of dynamic bonds (healing efficiency: 79.8% (25 °C), Fig. 3a). The unique dipole–dipole interactions in polymer matrixes thus could on-demand implement self-healing. We thus employed three samples (**P1**, **P2**, **P3**) to create a self-healing sample for evaluating the self-healing ability (Fig. 3b).
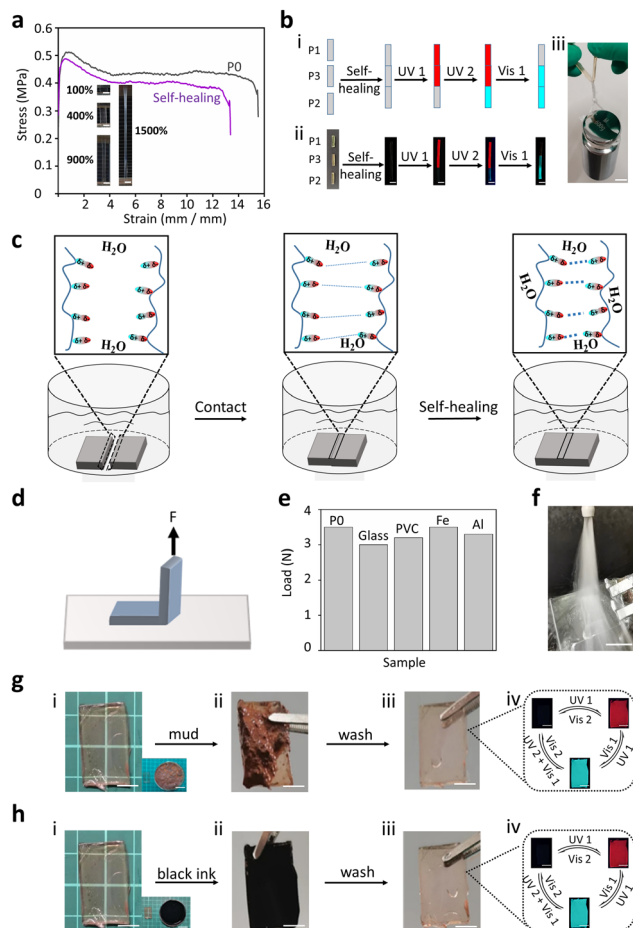
Fig. 3 Mechanical and self-healing properties, adhesion and antifouling. (a) Stress−strain curves of **P0** and self-healing sample. Inset in (a): Optical photographs of a product (**P0**) at different stretching states (100%, 400%, 900%, 1500%). (b) Self-healing performance demonstration. (i) Schematic illustration of the self-healing process using **P1**, **P2**, and **P3**. (ii) Photos showing the self-healing process. (iii) The self-healing sample bearing a weight (500 g). (c) Schematic illustration of the self-healing process. (d) Schematic diagram of the adhesion energy test. (e) Adhesion test of **P0** on different material surfaces (Glass, PVC, Iron, Aluminum). (f) Photograph showing the adhesion performance of **P0** under water flow blasting for 5 min. Anti-fouling property of **P3** after soaking in mud (g) and black ink (h) for one week, and the photochromic display. (i) Original samples; (ii) original samples immersed into the correspond medium for one week; (iii) contaminated samples washed *via* water; (iv) fluorescence variation of clean **P3** film after irradiation with different UV (UV1 and UV2) and Vis (Vis1 and Vis2). All scale bars are 1.0 cm.

As revealed in Fig. 3b, when the samples were healed under water for 24 h, the healed sample containing **P1**, **P2** and **P3** not only showed outstanding photoswitchable properties but also lifted 200 times its own weight (500 g). This sample could be stretched well without breaking, and exhibited fluorescent properties under UV light (Fig. S13, ESI†). Such excellent underwater self-healing performance should be attributed to the fact that the dipole–dipole interactions can lock the interfaces in contact with each other (Fig. 3c). We also investigated its adhesion ability to different substrates (Glass, PMMA, sheet iron, aluminium sheet) using a stripping method (Fig. 3d). The

polymers are polymerized directly to the surface of the corresponding materials. The results exhibited that its adhesion is greater than its fracture energy (> 3.5 N, Fig. 3e, and Fig. S14, ESI†), demonstrating the application potential of **PSFPs** in anti-counterfeiting labels. As shown in Fig. 3f, samples (**P0**) attached to the glass will not fall off under the impact of high-speed water flow (> 16 L min^{-1}, Video S1). In addition, the non-covalent crosslinking supramolecular interaction can endow the material with eminent processability. We thus evaluated the processability of **PSFPs** (**P0**) through solvent and heat. The cuboid sample can be transformed into a triangular body by cutting and subsequent reprocessing with solvent (THF, Fig. S15, ESI†). This shape was further transformed into a pentagonal sample by heat treatment (100 °C). These results demonstrated that **PSFPs** present the desired self-healing and processability. Such features could ensure that **PSFPs** have good application prospects in information encryption and anti-counterfeiting labels with self-healing ability.

The dipole–dipole interactions ensured that the **PSFPs** exhibited hydrophobicity (water contact angle (WCA) > 115°, Fig. S16, ESI†) and chemical stability in aqueous conditions because of the weak hydrogen bond acceptance of the C–F bond.[57] This feature would make the material have good self-cleaning properties. **P3** was first immersed into the mud for a week. As seen in Fig. 3g, when the samples stained by sludge were simply cleaned with water, all the remaining stains were completely removed. The cleaned sample (**P3**) still showed satisfactory photo-response properties. A similar result could be observed by immersing **P3** in black ink for a week (Fig. 3h), indicating that the sample has well-pleasing antifouling ability. Furthermore, the exceptional environmental stability including salt, acid and alkali resistance was also explored. The **P3** was soaked into the different solutions (pure water (pH = 7.05), acid solution (HCl, pH = 1), basic solution (NaOH, pH = 14), and salt solution (26.5 wt%, seawater)). Even when stored in these environments for more than a week, no significant change in the photoswitchable ability and weight was observed (Fig. S17–S19, ESI†). In addition, a negligible change in the fluorescence quantum yields of P1, P2, and P3 under ambient conditions and in water also supports this conclusion (Table S2, ESI†). These characteristics enabled us to apply **PSFPs** in underwater information encryption and anti-counterfeiting labels.

Based on the above-mentioned features, **PSFPs** were further applied to constructing information encryption systems. We first make the polymer (**P0**: dye-free; **P1**: including BTBA units; **P2**: including SDTE units; **P3**: including BTBA and SDTE units) into the corresponding information encryption boxes. **P0** boxes served as a no information carrier, and **P1**, **P2**, and **P3** boxes acted as carriers of primary information, secondary information and tertiary information. These boxes are bonded together under water to form a complete rectangle block (Fig. 4a). The on-demand multilevel information could be integrated into the polymer block (Fig. 4a). Among them, **P3** boxes were utilized to serve as an independent encryption unit and an information jamming unit. As depicted in Fig. 4b and c, the encrypted information combining with **P1**, **P2**, and **P3** ("89") can be
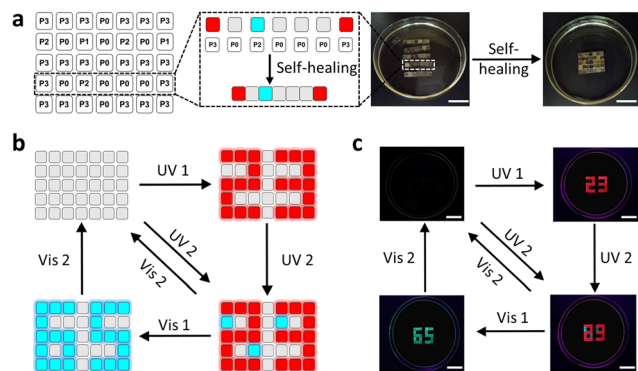
Fig. 4 Demonstrated models for applying PSFPs in information encryption. (a) The preparation of the encryption model and the corresponding photographs using **P0**, **P1**, **P2**, and **P3**. (b) Schematic diagram of the information decryption process under different wavelength light irradiation. (c) Optical photographs of the information decryption process under different wavelength light irradiation. All scale bars are 1.0 cm.

decrypted *via* UV2, and then be re-encrypted using Vis 2. When the UV1 and Vis 1 were further introduced, the encrypted information ("23", "89", and "65") appeared and disappeared one by one form "23" to "89" and "65", and eventually returning to their original state (Fig. 4c). This result indicated that **PSFPs** could be utilized to create on-demand multilevel information encryption systems.

In daily life, anti-counterfeiting labels are a very important anti-counterfeiting means to identify counterfeit and shoddy products.[59,60] Multilevel information decrypted by multiple means is necessary to improve information security and prevent copying. Moreover, underwater anti-counterfeiting labels often have to be used in harsh environments such as high salt concentrations, which require materials with better properties. Therefore, thanks to their excellent properties, including fast photo-responsibility, prominent photo-reversibility, antifouling, self-healing ability, simple preparation process, and processability, **PSFPs** were a desired platform for creating underwater anti-counterfeiting labels. We thus fabricate an artificial butterflyfish as an anti-counterfeiting label to evaluate the underwater applicability of **PSFPs**. As shown in Fig. 5a, we divided the butterflyfish into seven parts (A1–A7). The seven corresponding polymers with different proportions of dyes (BTBA/SDTE:2/0-0/2) were synthesized (Fig. 5a). Briefly, A1 only contained BTBA, and served as a fish's tail. The content of BTBA was gradually decreased from A2 to A6. A7 only included SDTE. Finally, the as-prepared parts are pieced together, and healed into an artificial butterflyfish under water (Fig. 5a). The artificial butterflyfish showed a distinct gradient of fluorescence (red to green) from the tail to the head. Fig. 5b and c shows the schematic diagram and optical photographs of the photoswitchable discoloration process, respectively. It's non-fluorescent in its initial state. When the artificial butterflyfish were irradiated by 365 nm UV, red fluorescence occurred. Subsequently, UV (254 nm) would trigger a change in green fluorescence. Next, the red and green fluorescence were gradually faded by the stimulation of Vis1 (525 nm) and Vis2
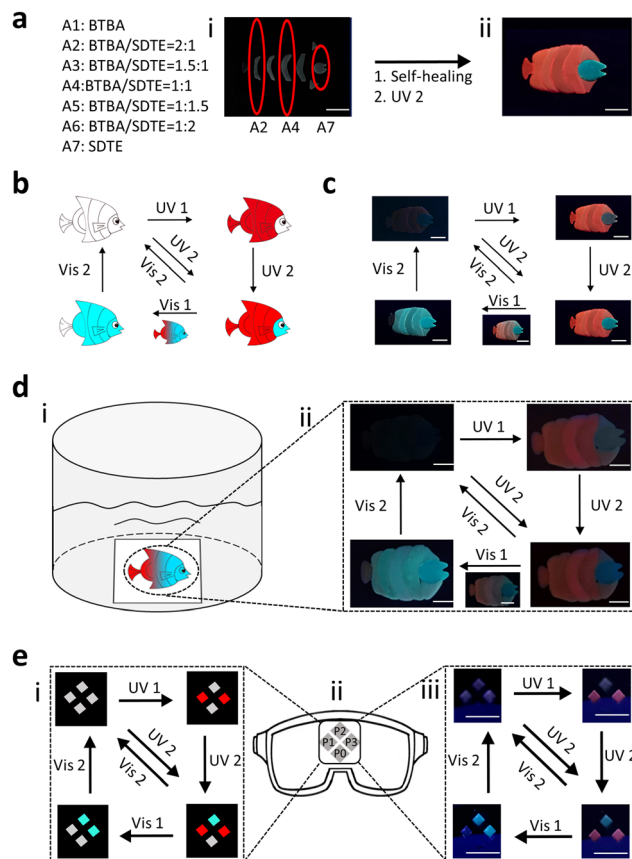

Fig. 5 Anti-counterfeiting label application design model and optical photos. (a) Preparation diagram of a fish-shaped anti-counterfeiting label and corresponding ingredients. Optical photographs of the fish-shaped anti-counterfeiting label before (i) and after (ii) self-healing. (b) Schematic diagram of the photoswitchable fluorescence of the fish-shaped anti-counterfeiting label. (c) Optical photographs of the photoswitchable fluorescence of the fish-shaped anti-counterfeiting label. (d) Light-induced photochromic processes of the fish-shaped anti-counterfeiting label adhering to glass under water. (i) Schematic diagram of the test device; (ii) underwater optical photographs of the photoswitchable fluorescence of the fish-shaped anti-counterfeiting label. (e) Anti-counterfeiting label displayed in diving goggles. (i) Schematic diagram of the photoswitchable fluorescence of the anti-counterfeiting label. (ii) Schematic diagram of the test device; (iii) underwater optical photographs of the photoswitchable fluorescence of anti-counterfeiting label. All scale bars are 1.0 cm.

(460 nm), respectively. Finally, the artificial butterflyfish changes to its initial non-fluorescence state. To further demonstrate the spatial-controllability of this process, we simulated an underwater environment to explore this performance (Fig. S20, ESI†). As illustrated in Fig. 5d, the artificial butterflyfish is posted on a glass plate as an anti-counterfeiting label, exhibiting a non-fluorescent state under a 365 nm UV lamp. By employing UV (254 nm and 365 nm) to irradiate the artificial butterflyfish, non-fluorescent butterflyfish were converted into a fluorescent state. Subsequently, Vis light was chosen to illuminate the fluorescent state of the butterflyfish to adapt and blend in with the new environment. This process can be implemented underwater. These results demonstrated that

PSFPs with a spatial-controlled photo-response were an ideal platform for creating underwater anti-counterfeiting labels and information encryption systems.

In addition, swimming equipment, especially ocean diving equipment, has higher requirements for anti-counterfeiting labels because of the harsh environment. The anti-counterfeiting labels in diving goggles were fabricated using **PSFPs** (**P0**, **P1**, **P2**, and **P3** and Fig. S21, ESI†). As indicated in Fig. 5e, the non-fluorescence state of the anti-counterfeiting labels could be converted into a different form by combining different light (UV1, UV2, Vis1, and Vis2). Briefly, UV1 drives **P1** and **P3** to display information, UV2 prompts **P2** to exhibit all information, Vis1 erases part of the displayed information from **P1** and **P3**, and Vis2 eliminates all information. In this process, reversible multi-state fluorescence changes can be achieved by using different light to stimulate the anti-counterfeiting labels, indicating the application potential and advantage of **PSFPs** in underwater anti-counterfeiting labels.

Conclusions

In summary, we have successfully prepared **PSFPs** *via* the copolymerization of diarylethylene derivatives (BTBA, SDTE), and fluorinated acrylate (TFEMA, HFBA). Thanks to the satisfying stability of dipole–dipole interactions based on strong molecular dipole and the photoswitchable performance of diarylethylene derivatives, the as-prepared **PSFPs** not only displayed outstanding photoreversibility, and eminent photostability, but also showed excellent self-healing ability, stretchability, hydrophobicity, antifouling, and exceptional environmental stability including salt, acid and alkali resistance. We thus successfully implemented **PSFPs** in underwater light-induced adaptive discoloration like butterflyfish, information encryption and anti-counterfeiting labels. Therefore, we anticipate their potential applications for anti-counterfeiting labels in harsh underwater environments.

Experimental

Preparation of PSFPs

Taking **P3** as an example: the solution of TFEMA (10 mmol) and HFBA (10 mmol) containing I-819 (0.2 mmol), BTBA (8.18 × 10^{-2} mmol), and SDTE (6.36 × 10^{-2} mmol) was irradiated by Vis light (460 nm, 40 mW cm^{-2}) for 1 h in reaction cells consisting of a pair of glass plates with 0.8 mm spacing to get polymers (**P3**). For other samples containing BTBA or SDTE, detailed sample information can be found in Table S1 (ESI†).

Preparation of films

The obtained polymers **P0**, **P1**, **P2** and **P3** were dissolved in dichloromethane, and after ultrasonic treatment for 5 min, a polymer solution of 30 mg mL^{-1} was obtained. The transparent solution was added dropwise to a clean glass substrate (Piranha solution as washing agent) and dried overnight at room temperature to obtain the fluorescent films.

Author contributions

Haitao Deng: conceptualization, methodology, investigation, validation, formal analysis, writing – original draft, writing – review & editing. Hong Wang: conceptualization, methodology, investigation, validation, formal analysis, supervision, writing – original draft, writing – review & editing. Yong Tian: formal analysis, writing – review & editing. Zhong Lin: formal analysis, writing – review & editing. Jiaxi Cui: conceptualization, methodology, formal analysis, supervision, writing – original draft, writing – review & editing, funding acquisition. Jian Chen: conceptualization, methodology, formal analysis, supervision, writing – original draft, writing – review & editing, funding acquisition.

Conflicts of interest

There are no conflicts of interest to declare.

Acknowledgements

Notes and references

1 Q. Zhang, W. Wang, C. Cai, S. Wu, J. Li, F. Li and S. Dong, *Mater. Horiz.*, 2022, **9**, 1984–1991.

2 T.-P. Huynh, M. Khatib and H. Haick, *Adv. Mater. Technol.*, 2019, **4**, 1900081.

3 H. Zhang, J. He and J. Qu, *Eur. Polym. J.*, 2022, **178**, 111487.

4 J. Liu, X. Li, K. Chen, Y. Li, S. Feng, P. Su, Y. Zou, Y. Li and W. Wang, *Macromol. Rapid Commun.*, 2023, DOI: **10.1002/marc.202300282**.

5 Y. Sun, X. Le, S. Zhou and T. Chen, *Adv. Mater.*, 2022, **34**, e2201262.

6 C. Liu, A. K. Steppert, Y. Liu, P. Weis, J. Hu, C. Nie, W. C. Xu, A. J. C. Kuehne and S. Wu, *Adv. Mater.*, 2023, **35**, 202303120.

7 J. Ma, Y. Yang, C. Valenzuela, X. Zhang, L. Wang and W. Feng, *Angew. Chem., Int. Ed.*, 2022, **61**, e202116219.

8 F. Xu and B. L. Feringa, *Adv. Mater.*, 2023, **35**, e2204413.

9 T. Fukaminato, T. Umemoto, Y. Iwata, S. Yokojima, M. Yoneyama, S. Nakamura and M. Irie, *J. Am. Chem. Soc.*, 2007, **129**, 5932–5938.

10 L. Kortekaas and W. R. Browne, *Chem. Soc. Rev.*, 2021, **50**, 2211.

11 C. Li, H. Yan, L.-X. Zhao, G.-F. Zhang, Z. Hu, Z.-L. Huang and M.-Q. Zhu, *Nat. Commun.*, 2014, **5**, 5709.

12 W. Hu, C. Sun, Y. Ren, S. Qin, Y. Shao, L. Zhang, Y. Wu, Q. Wang, H. Yang and D. Yang, *Angew. Chem., Int. Ed.*, 2021, **60**, 19406–19412.

13 M. Chen, B. Yao, M. Kappl, S. Liu, J. Yuan, R. Berger, F. Zhang, H. J. Butt, Y. Liu and S. Wu, *Adv. Funct. Mater.*, 2019, **30**, 1906752.

14 Z. Zhang, W. Wang, P. Jin, J. Xue, L. Sun, J. Huang, J. Zhang and H. Tian, *Nat. Commun.*, 2019, **10**, 4232.

15 S. Lin, K. G. Gutierrez-Cuevas, X. Zhang, J. Guo and Q. Li, *Adv. Funct. Mater.*, 2020, **31**, 2007957.

16 J. Jiang, Q. Chen, M. Xu, J. Chen and S. Wu, *Macromol. Rapid Commun.*, 2023, **44**, e2300117.

17 M. C. Baier, J. Huber and S. Mecking, *J. Am. Chem. Soc.*, 2009, **131**, 14267–14273.

18 W. R. Algar, M. Massey, K. Rees, R. Higgins, K. D. Krause, G. H. Darwish, W. J. Peveler, Z. Xiao, H.-Y. Tsai, R. Gupta, K. Lix, M. V. Tran and H. Kim, *Chem. Rev.*, 2021, **121**, 9243–9358.

19 K. K. Ng and G. Zheng, *Chem. Rev.*, 2015, **115**, 11012–11042.

20 Z. Lin, H. Wang, M. Yu, X. Guo, C. Zhang, H. Deng, P. Zhang, S. Chen, R. Zeng, J. Cui and J. Chen, *J. Mater. Chem. C*, 2019, **7**, 11515–11521.

21 X. Xu, V. V. Jerca and R. Hoogenboom, *Mater. Horiz.*, 2021, **8**, 1173–1188.

22 Z. Wang, A. Li, Z. Zhao, T. Zhu, Q. Zhang, Y. Zhang, Y. Tan and W. Z. Yuan, *Adv. Mater.*, 2022, **34**, e2202182.

23 F. Luo, T. L. Sun, T. Nakajima, T. Kurokawa, Y. Zhao, K. Sato, A. B. Ihsan, X. Li, H. Guo and J. P. Gong, *Adv. Mater.*, 2015, **27**, 2722–2727.

24 X. Du, J. Zhou, J. Shi and B. Xu, *Chem. Rev.*, 2015, **115**, 13165–13307.

25 H. Wang, C. N. Zhu, H. Zeng, X. Ji, T. Xie, X. Yan, Z. L. Wu and F. Huang, *Adv. Mater.*, 2019, **31**, 1807328.

26 Y. Guo, J. Bae, Z. Fang, P. Li, F. Zhao and G. Yu, *Chem. Rev.*, 2020, **120**, 7642–7707.

27 H. Wang, X. Xiong, L. Yang, Y. Fang, J. Xue and J. Cui, *Adv. Funct. Mater.*, 2022, **33**, 2212402.

28 W. Lu, X. Le, J. Zhang, Y. Huang and T. Chen, *Chem. Soc. Rev.*, 2017, **46**, 1284–1294.

29 R. Cheng, M. Xu, X. Zhang, J. Jiang, Q. Zhang and Y. Zhao, *Angew. Chem., Int. Ed.*, 2023, **62**, e202302900.

30 L. Li, W. Li, X. Wang, X. Zou, S. Zheng, Z. Liu, Q. Li, Q. Xia and F. Yan, *Angew. Chem., Int. Ed.*, 2022, **61**, e202212512.

31 B. J. Cafferty, R. R. Avirah, G. B. Schuster and N. V. Hud, *Chem. Sci.*, 2014, **5**, 4681–4686.

32 P. R. A. Chivers and D. K. Smith, *Nat. Rev. Mater.*, 2019, **4**, 463–478.

33 Z. Sun, F. Lv, L. Cao, L. Liu, Y. Zhang and Z. Lu, *Angew. Chem., Int. Ed.*, 2015, **54**, 7944–7948.

34 D. B. Amabilino, D. K. Smith and J. W. Steed, *Chem. Soc. Rev.*, 2017, **46**, 2404–2420.

35 X.-L. Ni, X. Xiao, H. Cong, Q.-J. Zhu, S.-F. Xue and Z. Tao, *Acc. Chem. Res.*, 2014, **47**, 1386–1395.

36 W. Han, W. Xiang, Q. Li, H. Zhang, Y. Yang, J. Shi, Y. Ji, S. Wang, X. Ji, N. M. Khashab and J. L. Sessler, *Chem. Soc. Rev.*, 2021, **50**, 10025–10043.

37 H. Chen and J. Fraser Stoddart, *Nat. Rev. Mater.*, 2021, **6**, 804–828.

38 S. J. D. Lugger, S. J. A. Houben, Y. Foelen, M. G. Debije, A. Schenning and D. J. Mulder, *Chem. Rev.*, 2022, **122**, 4946–4975.

39 P. Sun, B. Qin, J.-F. Xu and X. Zhang, *Prog. Polym. Sci.*, 2022, **124**, 101486.

40 X. N. Zhang, C. Du, Y. J. Wang, L. X. Hou, M. Du, Q. Zheng and Z. L. Wu, *Macromolecules*, 2022, **55**, 7512–7525.

41 Y. Liu, J. Wan, X. Zhao, J. Zhao, Y. Guo, R. Bai, Z. Zhang, W. Yu, H. W. Gibson and X. Yan, *Angew. Chem., Int. Ed.*, 2023, **62**, e202302370.

42 S. Chen, Z. Li, C. Zhang, X. Wu, W. Wang, Q. Huang, W. Chen, J. Shi and D. Yuan, *Small*, 2023, **19**, e2301063.

43 S. J. D. Lugger, S. J. A. Houben, Y. Foelen, M. G. Debije, A. P. H. J. Schenning and D. J. Mulder, *Chem. Rev.*, 2022, **122**, 4946–4975.

44 H. Yang, S. Li, J. Zheng, G. Chen, W. Wang, Y. Miao, N. Zhu, Y. Cong and J. Fu, *Adv. Mater.*, 2023, DOI: **10.1002/adma.202301300**.

45 J. Tang, Y. Tian, Z. Lin, C. Zhang, P. Zhang, R. Zeng, S. Wu, X. Chen and J. Chen, *ACS Appl. Mater. Interfaces*, 2023, **15**, 2237–2245.

46 Z. Qin, Y. Yang, Q. Tian, H.-Y. Mi, H. Li, R. Guo, Y. Wang, C. Liu and C. Shen, *Chem. Eng. J.*, 2023, **467**, 143434.

47 N. M. Sangeetha and U. Maitra, *Chem. Soc. Rev.*, 2005, **34**, 821–836.

48 P. Wang, Q. Liao, B. Yuan and H. Zhang, *ACS Appl. Mater. Interfaces*, 2023, **15**, 32945–32956.

49 A. K. Chau and F. K. Leung, *Adv. Colloid Interface Sci.*, 2023, **315**, 102892.

50 D. Li, Z. Feng, Y. Han, C. Chen, Q.-W. Zhang and Y. Tian, *Adv. Sci.*, 2022, **9**, 2104790.

51 H. Wang, X. Ji, Z. Li and F. Huang, *Adv. Mater.*, 2017, **29**, 1606117.

52 Y. Liu, T. Chen, Z. Jin, M. Li, D. Zhang, L. Duan, Z. Zhao and C. Wang, *Nat. Commun.*, 2022, **13**, 1338.

53 J. Jiang, P. Zhang, Y. Tian, Z. Lin, C. Zhang, J. Cui, J. Chen and X. Chen, *Sci. China Mater.*, 2023, **66**, 1949–1958.

54 S. Wang and M. W. Urban, *Adv. Sci.*, 2021, **8**, 2101399.

55 A. M. C. Maan, A. H. Hofman, W. M. Vos and M. Kamperman, *Adv. Funct. Mater.*, 2020, **30**, 2000936.

56 Y. Jia, L. Zhang, M. Qin, Y. Li, S. Gu, Q. Guan and Z. You, *Chem. Eng. J.*, 2022, **430**, 133081.

57 S. Huang, Y. Wan, X. Ming, J. Zhou, M. Zhou, H. Chen, Q. Zhang and S. Zhu, *ACS Appl. Mater. Interfaces*, 2021, **13**, 41112–41119.

58 F. Nonque, A. Benlahoues, J. Audourenc, A. Sahut, R. Saint-Loup, P. Woisel and J. Potier, *Eur. Polym. J.*, 2021, **160**, 110799.

59 A. O. Larin, L. N. Dvoretckaia, A. M. Mozharov, I. S. Mukhin, A. B. Cherepakhin, I. I. Shishkin, E. I. Ageev and D. A. Zuev, *Adv. Mater.*, 2021, **33**, e2005886.

60 J. Zhang, Y. Liu, C. Njel, S. Ronneberger, N. V. Tarakina and F. F. Loeffler, *Nat. Nanotechnol.*, 2023, **18**, 1027–1035.